Tellus (1996), 48A, 622–643
Printed in UK – all rights reserved

TELLUS
ISSN 0280-6495

Simulating the Baltic Sea ice season with a coupled ice-ocean model

By JARI HAAPALA* and MATTI LEPPÄRANTA *Department of Geophysics, P.O. Box 4 (Fabianinkatu 24A), 00014 University of Helsinki, Finland*

(Manuscript received 10 November, 1995; in final form 13 June 1996

ABSTRACT

The Baltic Sea ice season climatology is studied with a coupled ice-ocean model. The evolution of sea temperature, ice thickness and ice drift has been simulated for three particular ice seasons, normal (1983/84), severe (1986/87) and mild (1991/92), forced with the prescribed daily atmospheric data. The ice model is a plastic Hibler model with a three-level ice thickness distribution (open water, undeformed ice and ridged ice) and thermodynamics. The ocean model consists of a barotropic circulation model with 4-layer vertical thermodynamic evolution. The models are coupled via the momentum and heat fluxes; the grid size is 10′ in latitude and 20′ in longitude. With the same initial conditions and observed meteorological forcing, a fully prognostic thirteen-months integration was performed for each ice season from 1 May to 31 May in the following year. The model results were compared with routine ice charts. The annual cycles of sea surface temperature, ice thickness and coverage, and the interannual variability of the ice seasons were realistically simulated. Ocean surface temperatures were produced well in the shallow sea areas, but over the deeper central parts of the basins they were too warm in the winter stage. On the average and severe winters the predicted maximum ice extent was about 20% less than that observed, while in the mild winter the agreement was very good. Basin scale features were rather well realized in the ice thickness field. The freezing date and ice growth were in agreement with observations, but the beginning of the ice melting was delayed which led to about 1–2 weeks delay in the ice break-up date.

1. Introduction

The seasonal sea ice cover is an essential feature of the Baltic Sea. The ice season normally lasts 5–7 months, from November to May, i.e., in the northern parts of the Baltic the ice covered period is even longer than the ice-free season. The year-to-year variability of the ice seasons is large. During a mild winter, ice only occurs in the Bothnian Bay, but in a cold winter the whole Baltic Sea becomes ice-covered (Fig. 1).

From the geophysical point of view, sea ice is a thin and rather rigid film of complex morphology at the ocean-atmosphere interface. Ice largely modifies or even eliminates the ocean-atmosphere heat, radiation and momentum fluxes. The albedo and surface roughness of the ice are different than those of open water. An ice pack also holds and advects fresh water, heat, atmospheric settling and sediments, and may release them far away from the source. An essential difference between ice dynamics and ocean and atmosphere dynamics is that drift ice shows a nonlinear plastic behavior with a large part of the mechanical energy consumed in irreversible internal deformation processes like ridging and rafting. The atmosphere and ocean are always in motion but an ice field may be static. The Bothnian Bay observations show that the ice pack may be motionless even during a strong (15 ms^{-1}) wind.

* Corresponding author.
Jari.J.Haapala@Helsinki.Fi

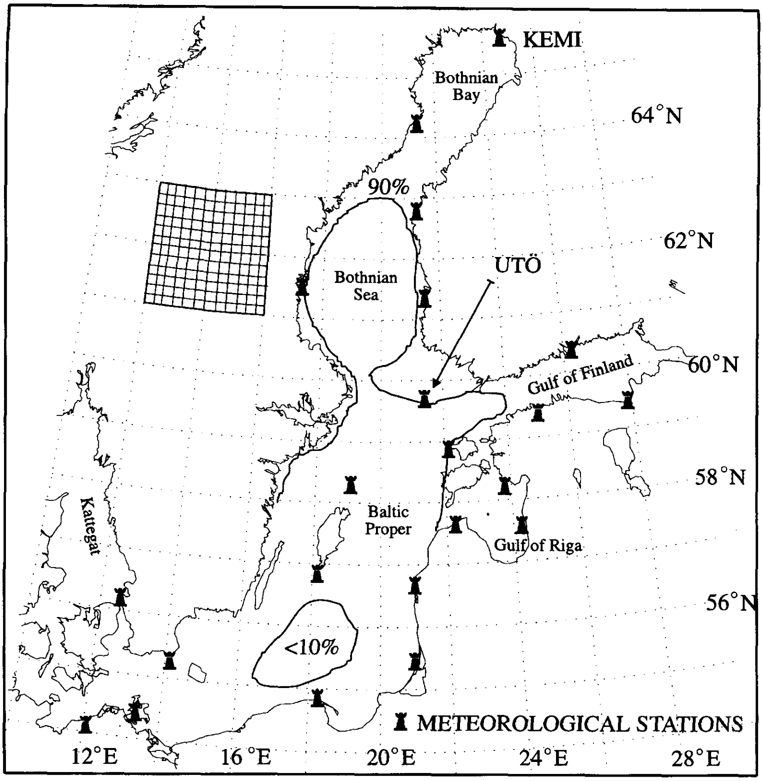

Fig. 1. The Baltic Sea and the coastal meteorological stations used for the model forcing. The solid lines indicate probabilities of ice occurrence of 10 and 90% (SMHI and FIMR, 1982). The grid size is illustrated on the left side.

The present approach to model meso- and large-scale ice dynamics is to comprehend the ice pack as a continuum (Hibler, 1986). The main problem is to determine the internal ice stress, which arises from ice floe interactions. Hibler (1979) proposed a viscous-plastic sea ice rheology, when modelling the large-scale ice motion of the Arctic. That work has also been used in several coupled ice-ocean models for coastal seas (Ikeda 1988; Kantha and Mellor, 1989) and in other developments (Overland and Pease, 1988). Although seasonal studies of the whole Arctic have been carried out intensively, coastal and marginal seas have received less attention. Recently, Wang et al. (1994a) have modelled and examined the seasonal evolution of the sea ice characteristics of Hudson Bay. In the Baltic Sea Omstedt and Nyberg (1996) have performed the first decade-scale simulations with a one-dimensional coupled ice-ocean model. Two-dimensional coupled ice-ocean models have been used for rather short-duration simulations in ice forecasting (Omstedt et al., 1994) and dynamics research (Zhang and Leppäranta, 1995).

This paper presents a new seasonal ice-ocean model for the Baltic Sea and shows the simulation results for three specific ice seasons. First the physics of the ice and ocean models is set out and the coupling of the models is introduced. Three particular ice seasons have been selected to represent normal (1983/84), severe (1986/87) and mild (1991/92) case; these are briefly described in Section 3. The model's ability to reproduce seasonal ice characteristics and the main simulation results are presented in Section 4, and finally the conclusions are given in Section 5.

2. Description of the model

The evolution of the ice season is driven by the atmospheric and oceanic forcing and radiation.

The ice drift is mainly driven by the wind, while the air temperature basically determines the ice growth. The rôle of the Baltic water masses is to store heat and consequently delay freezing, and to provide the friction for the ice motion. On a seasonal scale the ice and ocean are highly coupled. The evolution of the ice conditions depends on the heat which was stored in the sea during the previous summer and autumn. In turn, the ice pack modifies the momentum, heat and salt balance of the sea.

Here a new coupled ice-ocean model has been developed for research into the Baltic Sea ice season. The requirements were to reproduce realistic growth, decay, and drift of the ice, as well as pack ice ridging and opening processes. The main oceanic processes for controlling the ice season evolution were considered as the vertical mixing, the heat transport at sea surface and the horizontal advection of heat. The present model includes, for the ice, full dynamics and thermodynamics, and, for the sea water, two-dimensional barotropic dynamics and thermodynamics in 3 dimensions. The ocean model neglects three factors—baroclinic circulation, water exchange between the North Sea and the Baltic and the effect of river runoff — which are thought to be meaningful in the ice season problem and will be considered in the further development of the present model.

2.1. Ice model

The ice model consists of the momentum balance, the constitutive law, the conservation law of ice thickness and compactness (ice concentration), and heat budget (Semtner, 1976; Hibler, 1979; Leppäranta, 1981a). Prognostic variables are ice thickness, compactness, temperature and velocity. Some simplification of Hibler's model has been made. In the Baltic, nonlinear advective terms are insignificant. Also sea-surface slope can be neglected from the momentum balance, because the slope term/Coriolis term ratio is equal to the geostrophic current/ice velocity ratio which is generally <0.3; also note that the Coriolis term is much smaller than the wind stress as the ice is thin (Leppäranta, 1981b). The momentum balance for the horizontal ice flow then reads

$$\rho_i h_i^m \frac{\partial \boldsymbol{u}_i}{\partial t} = -\rho_i h_i^m f \hat{\boldsymbol{k}} \times \boldsymbol{u}_i + \boldsymbol{\tau}_{ai} + \boldsymbol{\tau}_{wi} + \nabla \cdot \sigma \qquad (1)$$

Here ρ_i is the ice density, h_i^m is the mean ice thickness, $\boldsymbol{u}_i$ is the ice velocity vector, t is the time, f is the Coriolis parameter, $\hat{\boldsymbol{k}}$ is the unit vector vertically upward, $\boldsymbol{\tau}_{ai}$ and $\boldsymbol{\tau}_{wi}$ are the air and water stresses, and σ is the ice stress tensor. The ice internal stress obeys the nonlinear viscous-plastic constitutive law of Hibler (1979)

$$\sigma = 2\eta\dot{\varepsilon} + (\zeta - \eta)\,\mathrm{tr}\,\dot{\varepsilon}\boldsymbol{I} - \tfrac{1}{2}P\boldsymbol{I}, \qquad (2)$$

where $\dot{\varepsilon}$ is strain rate tensor, ζ and η are nonlinear bulk and shear viscosities, $\boldsymbol{I}$ is the unit tensor and P the ice strength. For plastic flow the viscosities are determined on the basis of the normal flow rule on an elliptical yield curve located in the third quadrant in principal stress space; in a very slow deformation, the viscosities are constants, producing a linear viscous behavior (for details, see Hibler, 1979). The exact yield curve shape is determined by the aspect ratio $e^2 = \zeta/\eta$. The ice strength links ice dynamics to ice thickness and compactness as follows

$$P = (P^* h_i^m) e^{-C(1-A)}, \qquad (3)$$

where P^* and C are empirical constants, P^* is the strength of a compact ice pack with unit thickness and $1/C$ is the e-folding scale of the stress reduction in opening. For the Baltic Sea we have used $P^* = 2.5 \cdot 10^4\ \mathrm{Nm}^{-2}$ found from a comparison of model velocity fields to ERS-1 SAR velocity fields (Leppäranta et al., 1995), while $C = 20$ and $e = 2.0$ were taken from the original work of Hibler (1979). The viscous-plastic transition is described by a fixed maximum bulk viscosity ζ_{max} which was set here to be $1 \cdot 10^{12}\ \mathrm{Nm}^{-2}\,\mathrm{s}^{-1}$.

The mass conservation law is decomposed into conservation equations for the evolution of the thickness of level ice h_i^l and ridged ice h_i^r and ice compactness A:

$$\frac{\partial}{\partial t}(h_i^l, h_i^r, A) = -\boldsymbol{u} \cdot \nabla (h_i^l, h_i^r, A) + (0, \Psi_r, \Psi_A) + (\Phi_l, \Phi_r, \Phi_A) + \text{diffusion}, \qquad (4)$$

where the terms on the right hand-side describe advection, mechanical thickness redistribution, thermodynamic effects and diffusion. The diffusion is used to eliminate the numerical instabilities. Hibler (1979) used both harmonic and biharmonic diffusion terms, here only the harmonic diffusion was used (Table 1). The deformation functions are similar to those given by Leppäranta (1981a) and Zhang and Leppäranta (1995); however, rafting is not taken into account. Two different types of deformation may occur. When the compactness is below 100%, or under divergence, only compactness changes occur

$$\Psi_r = 0,$$

$$\Psi_A = -A\nabla\cdot\boldsymbol{u}. \tag{5a}$$

In a compact ice situation ($A = 100\%$) under convergence, ice undergoes ridging:

$$\Psi_r = -h_i^m \nabla\cdot\boldsymbol{u},$$

$$\Psi_A = 0. \tag{5b}$$

The cut-off thickness for level ice is 0.1 m, any ice thickness below that is considered as thin ice h_i^0. This ice class is classified dynamically as open water, but thermodynamically as level ice. The mean ice thickness (effective ice thickness) used in the ice dynamic calculations is defined as $h_i^m = h_i^l + h_i^r$.

The thermodynamic growth and melting of ice is calculated according to the Semtner zero-level model (Semtner, 1976). This is good approximation for the Baltic Sea because typically ice thickness is 10–50 cm and the maximum ice thickness is about one metre. The ice thickness evolution is governed by the heat fluxes at the ice/ocean and ice/atmosphere interfaces. Ice growth is calculated only at the bottom of the ice, but melting is also calculated at the top of the ice. Let F_i be the conductive heat flux in the ice and F_{wi} the heat flux from ocean to ice. Then the growth or melting at the bottom is

$$\Phi_h = \frac{\partial h_i}{\partial t} = \frac{F_i - F_{wi}}{\rho_i L}. \tag{6}$$

Here h_i is the actual ice floe thickness (depending on the situation h_i refers to the thin ice thickness or level ice thickness) and L is the latent heat. Surface melting occurs if the surface receives more heat than the conductive flux removes. First the snow layer is melted and after that surface melting of ice is calculated:

$$\Phi_h = \frac{\partial h_i}{\partial t} = \frac{F_{tot} - F_i}{\rho_i L}, \quad h_s = 0, \quad F_{tot} - F_i < 0, \tag{7}$$

where F_{tot} is the total heat flux at surface and h_s is the snow thickness. Since the bottom temperature is at the freezing point T_{fp}, the conductive heat flux through the ice and snow layers is:

$$F_i = \frac{k_i}{h_i + (k_i/k_s)h_s}(T_{fp} - T_0), \tag{8}$$

where k_i and k_s are the thermal conductivities of ice and snow, respectively. The surface temperature T_0 is obtained iteratively from the heat balance. The freezing-point temperature is determined according to Millero (1978)

$$T_{fp} = -0.0575S + 1.710523\cdot10^{-3}\,S^{3/2} - 2.154996\cdot10^{-4}\,S^2, \tag{9}$$

where S is the water salinity in (ppt). The snow thickness growth is determined from the meteorological precipitation observations ($h_s = (\rho_w/\rho_s)\cdot$precipitation). Four different surface albedo values are used, 0.87, 0.77, 0.7, 0.3 for snow, wet snow, ice and wet ice, respectively (Perovich, 1996). The wet snow and wet ice types are used when the snow/ice surface temperature is at the melting point.

In the model, the initial freezing begins when the temperature of the first model layer has been cooled to the freezing point temperature. Thin and level ice growth are calculated separately. First the thin ice growth is calculated (0–10 cm) and when the ice thickness is larger than 10 cm the thin ice mass is converted to the level ice. The initial and cut-off thickness of ice was set equal to 0.1 cm. During the ice cover periods the ocean surface layer may gain heat due to advection, vertical mixing and heat exchange with the atmosphere. In a compact ice situation ($A = 100\%$) all of this extra heat provides a water-ice heat flux and melts the ice at the bottom (eq. (6)). In a partial ice cover ($A < 100\%$), melting is performed immediately. The extra heat is used for floe side melting and consequently ice compactness decreases; the modelled mean floe thickness ($(h_i^l + h_i^r)/A$) is used in the computation.

2.2. *Ocean model*

In the ocean model part, we use the vertically-integrated equations of motion, the continuity equation, the equation of state, and the conservation equations for heat and salt. The prognostic variables are the vertically-averaged velocity vector, the water level elevation and the three-dimensional temperature and salinity distributions. Temperature and salinity are fully prognostic and thus they are not bound to the climatology at any level. The nonlinear advective terms and the atmospheric pressure gradient have been neglected from the momentum balance, yielding:

$$\frac{\partial \bar{\boldsymbol{u}}}{\partial t}+f\hat{\boldsymbol{k}}\times\bar{\boldsymbol{u}}=-g\nabla\xi+\frac{\boldsymbol{\tau}_{\rm s}}{\rho_{\rm o}D}-\frac{\boldsymbol{\tau}_{\rm b}}{\rho_{\rm o}D}+N_{\rm h}(\nabla^2\bar{\boldsymbol{u}}), \tag{10}$$

where $\rho_{\rm o}$ is the reference density of sea water, $\bar{\boldsymbol{u}}$ is the vertically-averaged velocity vector, g is the gravitational acceleration, ξ is the water level elevation, $\boldsymbol{\tau}_{\rm s}$ and $\boldsymbol{\tau}_{\rm b}$ are the stresses at the surface and bottom, D is the total depth (bottom depth + water level) and $N_{\rm h}$ is the horizontal eddy viscosity. The water level elevation is obtained from the continuity equation

$$\nabla\cdot(\bar{\boldsymbol{u}}D)+\frac{\partial\xi}{\partial t}=0 \tag{11}$$

The density is calculated according to the international equation of state of sea water (EOS80, Fofonoff, 1985). The effect of pressure is taken into account, although in the Baltic it is small. Formally,

$$\rho=\rho(T,S,p). \tag{12}$$

The equations of conservation for heat and salt are

$$\frac{\partial(T,S)}{\partial t}+\nabla\cdot(T,S)\bar{\boldsymbol{u}}=k_{\rm h}\nabla^2(T,S)+\frac{\partial}{\partial z}\left(k_{\rm v}\frac{\partial}{\partial z}(T,S)\right). \tag{13}$$

Here T is the sea-water temperature and S the salinity, $k_{\rm h}$ is the horizontal and $k_{\rm v}$ the vertical diffusion coefficient. The horizontal diffusivity was set to $2.5\cdot10^2$ m^2 s^{-1}.

The vertical structures of the temperature and salinity were calculated, although only the vertically-integrated current was solved. Vertical mixing was handled by a free convection scheme and a vertical diffusion equation. A constant diffusion coefficient was found to be too crude an approximation. Generally, the parametrization of the vertical diffusion is based on the Richardson number (c.f., Lehmann, 1995). That we could not utilize, because the model has no information about the vertical structure of the currents. Assuming that the surface stress is the main factor to drive the surface mixing a specific parametrization for the surface layer was made. The vertical diffusion coefficient was set to be dependent only on the surface stress. Temperature and salinity effects could also be large in the surface mixed layer (Omstedt et al., 1983), but detail description can be solved only with high vertical resolution models (Omstedt and Nyberg, 1996). However, the most important temperature and salinity effect is the convection caused by the buoyancy differences. That is taken account using the free convective scheme in the model. In deeper levels a Brunt-Väisälä frequency (N) dependent scheme (Stigebrandt, 1987) was applied. The full formula reads

$$k_{\rm v}=\begin{cases}(1+100|\boldsymbol{\tau}_{\rm s}|)\cdot10^{-4}\ \mathrm{m^2\ s^{-1}}, & \text{top layer,}\\ \alpha N^{-1}, & \text{other layers,}\end{cases} \tag{14}$$

where $\boldsymbol{\tau}_{\rm s}$ is the surface stress given in Nm^{-2}. In the ice-free period, $\boldsymbol{\tau}_{\rm s}$ is the pure wind stress while in the ice-covered period it is the combined effect of the wind and ice stresses (see eq. (15b) below). This parametrization scheme gives the diffusivity a range of 10^{-4} m^2 s^{-1} to 10^{-2} m^2 s^{-1} in the top layer and generates more mixing during the autumn and winter than in the summer period. Given $\alpha=2\cdot10^{-7}$ m^2 s^{-2} (Stigebrandt, 1987), the vertical diffusivity falls to between 10^{-5} m^2 s^{-1} and 10^{-6} m^2 s^{-1} in the deeper layers. To avoid numerical instabilities certain limits for $k_{\rm v}$ have to be set. The upper limit of $k_{\rm v}$ is $(\Delta z)^2/2\Delta t$ (Δz is the vertical grid size and Δt the time step), typically 10^{-3} m^2 s^{-1} to 10^{-1} m^2 s^{-1}. The minimum $k_{\rm v}$ was set to 10^{-7} m^2 s^{-1}.

2.3. *Coupling*

The ice model is coupled to the top layer of the ocean model via the fluxes of momentum and heat. The stresses at the ice-ocean interface then read

$$\boldsymbol{\tau}_{\rm wi}=\rho_{\rm w}C^{\rm d}_{\rm wi}|\bar{\boldsymbol{u}}_{\rm w}-\boldsymbol{u}_{\rm i}|(\bar{\boldsymbol{u}}_{\rm w}-\boldsymbol{u}_{\rm i}), \tag{15a}$$

$$\boldsymbol{\tau}_{\rm s}=(1-A)\boldsymbol{\tau}_{\rm aw}-A\boldsymbol{\tau}_{\rm wi}, \tag{15b}$$

where $C^{\rm d}_{\rm wi}$ is the water-ice drag coefficient and $\tau_{\rm aw}$ is the wind stress on the open ocean. The water-ice drag coefficient $C^{\rm d}_{\rm wi}$ was set to $3.5\cdot10^{-3}$ (Leppäranta and Omstedt, 1990). Note that the turning angle is zero in the ice-water stress. This is for simplicity as the real angle would lie between zero and 20° depending on the thickness of the surface layer. The choice does not affect very much on the results; in shallow areas zero is a very good value.

The heat exchange of the ice and ocean model has two alternatives. In a partial ice cover ($A<100\%$) the extra heat is immediately used for floe side melting. Consequently ice compactness decreases and the temperature of the first model layer cools. In a compact ice situations and in the fast ice region ($A=100\%$) the heat excess melts the ice at the bottom and provides a water-ice heat flux. The heat flux is calculated according to the bulk formula

$$F_{\mathrm{wi}}=(\rho c)_{\mathrm{w}}C^{\mathrm{h}}_{\mathrm{wi}}|\tilde{\boldsymbol{u}}_{\mathrm{w}}-\boldsymbol{u}_{\mathrm{i}}|(T_{\mathrm{w}}-T_{\mathrm{fp}}), \tag{16}$$

where c_{w} is the specific heat of sea water and $C^{\mathrm{h}}_{\mathrm{wi}}$ is the bulk heat transfer coefficient and T_{w} is the water temperature of the first model layer. The ice-ocean heat flux parametrization has been compared to more sophisticated turbulence model results and gives reasonable results with $C^{\mathrm{h}}_{\mathrm{wi}}=2.8\cdot10^{-4}$ (Omstedt and Wettlaufer, 1992). To also allow for some heat exchange in the fast ice areas and immobile conditions a minimum for the velocity difference was set to be 0.1 cm s^{-1}.

2.4. *External forcing and boundary conditions*

The model is forced by the fluxes of momentum, heat and radiation acting at the ice-atmosphere and ocean-atmosphere interfaces. These fluxes are calculated according to the commonly used methods (Maykut, 1986). The transfer coefficients were kept constant for two reasons: first to keep the forcing simple to clearly distinguish the role of the model physics and, secondly, the meteorological forcing data used are rather crude for the stability corrections. The wind stresses to the ice and the ocean surfaces are

$$\boldsymbol{\tau}_{\mathrm{ai}}=\rho_{\mathrm{a}}C^{\mathrm{d}}_{\mathrm{ai}}|\boldsymbol{U}|\boldsymbol{U}, \tag{17a}$$

$$\boldsymbol{\tau}_{\mathrm{aw}}=\rho_{\mathrm{a}}C^{\mathrm{d}}_{\mathrm{aw}}|\boldsymbol{U}|\boldsymbol{U}. \tag{17b}$$

Here $C^{\mathrm{d}}_{\mathrm{ai}}$ and $C^{\mathrm{d}}_{\mathrm{aw}}$ are the wind drag coefficients for the ice and water (Table 1), and $\boldsymbol{U}$ is the surface wind vector. Since the surface wind is used, the turning angle is zero. The bottom stress of the ocean model also follows a quadratic dependence on velocity:

$$\boldsymbol{\tau}_{\mathrm{b}}=\rho_{\mathrm{w}}C^{\mathrm{d}}_{\mathrm{wb}}|\tilde{\boldsymbol{u}}_{\mathrm{w}}|\tilde{\boldsymbol{u}}_{\mathrm{w}}, \tag{18}$$

where $C^{\mathrm{d}}_{\mathrm{wb}}$ is the bottom drag coefficient.

The turbulent and radiative fluxes at the surface are calculated separately for snow, ice and ocean surfaces. The total sum is

$$F_{\mathrm{tot}}=F_{\mathrm{sw}}+F_{\mathrm{lw}}+F_{\mathrm{sh}}+F_{\mathrm{lh}}, \tag{19}$$

where F_{sw}, F_{lw}, F_{sh} and F_{lh} are the net short-wave radiation, net long-wave radiation, and turbulent sensible and latent heat fluxes, respectively. The short-wave radiation is calculated according to astronomical and atmospheric correction functions (Iqbal, 1983; Reed, 1977), the long-wave radiation is obtained from a Brunt-type parametrization scheme (Budyko, 1974), and the bulk formulae were applied for the turbulent fluxes (Table 1). The total heat-flux sum provides the boundary condition for thermodynamic ice growth and melting (eqs. (6) and (7)). The boundary condition for the ocean temperature at the surface is

$$\rho_{\mathrm{w}}c_{\mathrm{w}}\frac{\partial T}{\partial z}=(1-A)F_{\mathrm{tot}} \tag{20}$$

Prescribing the atmosphere is a restriction. In particular the air temperature tends to guide the advance and retreat the ice edge. This question could be examined by introducing air-sea/ice coupling. Due the small size of the Baltic Sea it is anticipated that the modifications resulting from the coupling are not drastic.

Although the advection and vertical mixing of the ocean salinity were calculated, the salinity changes due to evaporation/precipitation, river runoff and water exchange between the Baltic and the North Sea were not taken into account.

The lateral boundaries are passive. The water velocity components normal to the wall are set to zero. An additional condition for the ice velocity is defined to describe fast ice. A fast ice region is assumed to exist if the bottom depth is equal to or below ten metres. At these grid points and in the lateral boundaries the ice velocity is set to zero. To avoid unrealistic ice mass propagation, the ice velocity near the ice edge was calculated as follows: at the ice edge the ice velocity was calculated normally, but the velocity at the nearest ice-free grid points was set to free drift velocity.

Table 1. *Model parameters*

Parameter	Symbol	Value
air density	ρ_a	$1.3\ \mathrm{kg\ m^{-3}}$
water reference density	ρ_0	$1000\ \mathrm{kg\ m^{-3}}$
ice density	ρ_i	$900\ \mathrm{kg\ m^{-3}}$
snow density	ρ_s	$300\ \mathrm{kg\ m^{-3}}$
ice strength	P^*	$2.5 \cdot 10^4\ \mathrm{N\ m^{-2}}$
strength reduction constant	C	20
yield curve aspect ratio	e	2.0
diffusion coefficient for ice		$0.004\ \Delta x\ \mathrm{m^2\ s^{-1}}$
cut-off thickness of ice	h_i^0	0.1 m
maximum bulk viscosity	ζ_{max}	$1 \cdot 10^{12}\ \mathrm{kg\ s^{-1}}$
latent heat of fusion	L	$333.5 \cdot 10^3\ \mathrm{J\ kg^{-1}}$
thermal conductivity of ice	k_i	$2.2\ \mathrm{W\ m^{-1}\ K^{-1}}$
thermal conductivity of snow	k_s	$0.3\ \mathrm{W\ m^{-1}\ K^{-1}}$
Coriolis parameter	f	$1.26 \cdot 10^{-4}\ \mathrm{s^{-1}}$
horizontal eddy viscosity	N_h	$1 \cdot 10^2\ \mathrm{m^2\ s^{-1}}$
horizontal diffusion	k_h	$2.5 \cdot 10^2\ \mathrm{m^2\ s^{-1}}$
air-ice drag coefficient	C_{ai}^d	$1.8 \cdot 10^{-3}$
air-water drag coefficient	C_{aw}^d	$1.2 \cdot 10^{-3}$
water-ice drag coefficient	C_{wi}^d	$3.5 \cdot 10^{-3}$
water-bottom drag coefficient	C_{wb}^d	$2.0 \cdot 10^{-3}$
water-ice heat transfer coefficient	C_{wi}^h	$2.8 \cdot 10^{-4}$
air-water heat transfer coefficient	C_{aw}^h	$1.3 \cdot 10^{-3}$
air-ice heat transfer coefficient	C_{ai}^h	$1.3 \cdot 10^{-3}$

At all other ice-free grid points the ice velocity was set to zero.

2.5. *Model numerics, forcing and initial conditions*

The model equations are solved in a staggered rectangular Eulerian grid by a finite difference technique. The ocean temperature, salinity, water level, the ice thickness and compactness and the viscosities are located at the middle of each cell (Fig. 2). The ocean velocity components are situated at the edges and the ice velocity and mass at the corner of the grid cell. The spatial arrangement is a combination of the Arakawa "B" and "C" grids, where the ice model variables are spaced according to the "B" grid and ocean variables on the "C" grid. The horizontal grid size is 10′ in latitude and 20′ in longitude and the grid covers the whole Baltic Sea. The western boundary is closed at the Skagerrak (9°30′E). Vertically the thermodynamics are solved in sigma coordinates. In these simulations four equally-spaced levels were used (0, 0.33, 0.66, 1). The model topography is based on the Institut für Ostseeforschung (IOW) database (Seifert and Kayser, 1995). A east-west cross section showing the model domain is shown in Fig. 3.

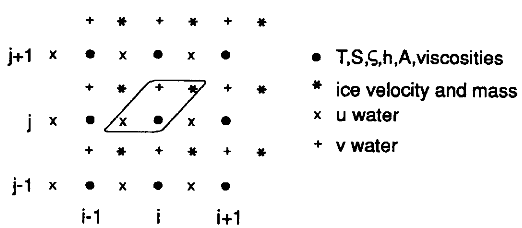

Fig. 2. The finite difference grid.

The ice momentum balance is solved for the ice velocities iteratively by overrelaxation, as introduced by Hibler (1979). A Fisher semi-implicit scheme of 2nd-order approximation in time and space was used for solving the ocean momentum balance (cf. Kowalik and Murty, 1993). The mass conservation equations are solved using the leapfrog method. The ice dynamics and thermodynamics are calculated with a 30-minute time step. The CFL (Courant-Friedrich-Levy) condition for gravity waves is about 300 s and accordingly the barotropic mode was solved with a 60-s time step. The ocean temperature and salinity advection and diffusion were calculated with a 30-min time step.

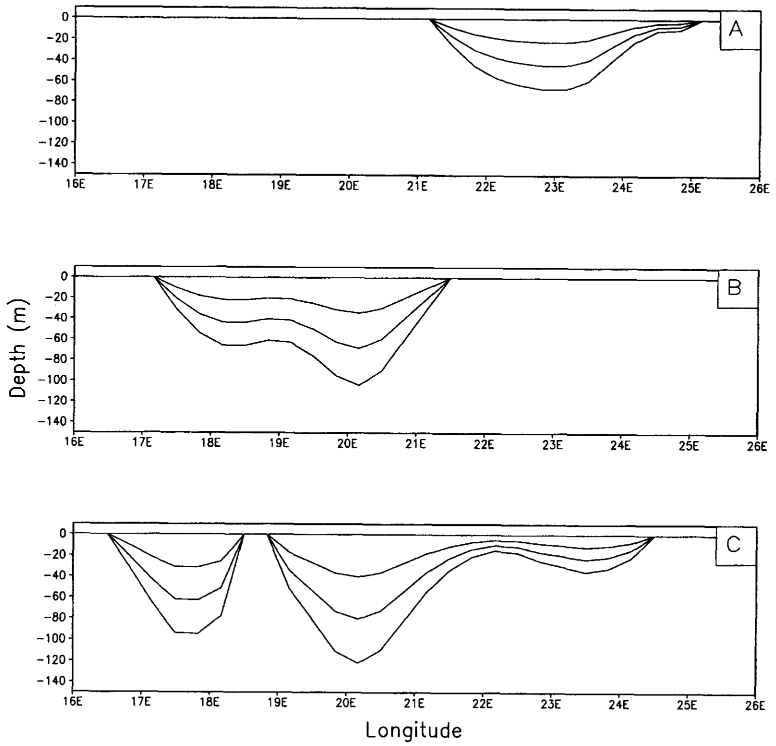

Fig. 3. Three east-west cross-sections of the model topography. The sigma-layers 0, 0.33, 0.66 and 1.0 are shown for the latitude 65°N (A) 62°N (B) and 57.75°N (C).

The model is forced via the fluxes of heat, moisture, radiation and momentum. The prescribed atmospheric conditions were produced from the daily observations of 22 coastal meteorological stations (Fig. 1). Data have been archived in the Baltic Sea Ice Climate Data Bank (Haapala et al., 1996). The data were linearly interpolated into the model grid from the three nearest stations. This simple interpolation is reasonable for the Central Baltic where stations exist both in the coastal areas and in the middle of the basin, but may be slightly biased in the Bothnian Bay and Bothnian Sea. For example, the wind velocity is usually greater in the open sea areas than in the coastal areas, and thus the method may underestimate the wind speed over the open ocean. The same interpolation method was used for constructing the initial conditions for the sea-water temperature and salinity from the 1961–90 climatology (Haapala and Alenius, 1994).

The model programme code is written in "c" and has been used in several platforms ranging from MS/DOS to supercomputers. Special attention has been paid to the code structure, modularity and efficiency. The code is freely available to the scientific community.

3. Characteristics of the ice seasons

The Baltic Sea is situated at latitudes where strong annual variations in all climatic quantities are typical. Observations of the thickness, extent and duration of the ice in the Baltic Sea also indicate a large interannual variability between the ice seasons (Alenius and Makkonen, 1981; Leppäranta and Seinä, 1985; Koslowski and Loewe, 1994). The ice season evolution is driven by the weather, ice/ocean interactions and the ice field internal processes. The main reason for this large natural variability is the sea's location between the North-Atlantic and Eurasian continental weather systems. The North Atlantic Oscillation (NAO) winter index has been widely used for describing large-scale air circulation patterns (Rogers, 1984) and has been related to sea ice characteristics in Hudson Bay and the Labrador Sea (Wang et al., 1994b; Mysak et al., 1996) and in the Baltic Sea (Koslowski and Loewe, 1994).

In this study, ice season characteristics have been examined for three particular winters. The ice seasons 1983/84, 1986/87 and 1991/92 have been selected as representing respectively normal, severe and mild winters; they have been selected as the references for Baltic ice climatological research (Haapala et al., 1996). The severe winter 1986/87 is also one of the BALTEX study periods (BALTEX, 1995). Some characteristic figures for these winters are given in Table 2.

Although the NAO index has a significant correlation with the ice season severity (Koslowski and Loewe, 1994), these three winters are not easily explained by the NAO index. NAO indexes for the winters 1983/84, 1986/87 and 1991/92 are 2.8, -1.2 and 1.0, respectively. Basically, large positive NAO indexes ($NAO > 1$) imply strong westerlies and mild ice winters and correspondingly large negative values ($NAO < -1$) weak westerlies and severe ice winters. Thus, according the NAO value the winter 1986/87 should have been severe and the winter 1991/92 mild as they were. However, even though strong westerlies prevailed during the winter 1983/84, the ice conditions in the Baltic were normal. As Koslowski and Loewe (1994) have pointed out, the NAO index gives only a rough estimate of the winter severity in the Baltic, but the specific air circulation patterns around the Baltic Sea are the determining factor in the evolution of the ice season.

The mean daily air temperatures for Kemi and Utö (Fig. 1) during the selected ice winters are shown in Fig. 4. The solid smooth line is the 1961–90 mean curve, the enveloping lines show the minimum and maximum values for this period, and the fluctuating solid line depicts the daily mean temperature for the selected seasons. The period is from the 1st September to the end of April in the following year. The general tendency of the temperature is similar at both stations; cold and warm periods are detectable in both time series.

The sum of negative degree-days gives an impression of the ice growth and the severity of the ice season. It is defined as (Maykut, 1986)

$$S = \int_0^t \max(0, T_{fp} - T_a)\,dt, \tag{21}$$

where T_{fp} is the freezing-point temperature and T_a the air temperature. The cumulative sums for Kemi and Utö are presented in Fig. 5. This shows

Table 2. *Characteristics of the observed and modelled ice seasons; observations are based on the FIMR's reports (Kalliosaari and Seinä, 1987; Seinä and Kalliosaari, 1991; Seinä, 1996)*

	Winter 1983/84		Winter 1986/87		Winter 1991/92	
Quantity	obs.	mod.	obs.	mod.	obs.	mod.
maximum ice extent (10^3 km^2)	187	156	405	331	66	64
occurrence of maximum ice extent	23 Mar	5 Apr	16 Mar	18 Mar	20 Feb	4 Mar
Kemi						
freezing date	4 Nov	11 Nov	2 Dec	5 Dec	18 Dec	14 Dec
max ice thickness (cm)	76	87	92	102	50	46
occurrence of max. thickness	17 Apr	3 Apr	14 Apr	20 Apr	10 Mar	18 Apr
break-up date	8 May	28 May	25 May	28 May	5 May	18 May
Utö						
freezing date	25 Jan/7 Mar[a]	11 Mar	3 Jan	8 Jan	no ice	no ice
max ice thickness (cm)	20–40[b]	27	69	34	–	–
occurrence of max. thickness	20–27 Mar[b]	25 Mar	7 Apr	6 Apr	–	–
break-up date	11 Apr	21 Apr	20 Apr	10 May	–	–

[a] The first freezing occurred 25 January 1984 and the formation of permanent ice occurred 7 March 1984.
[b] Ice thickness measurements were not made in Utö, these values are based on the nearest measurement sites.

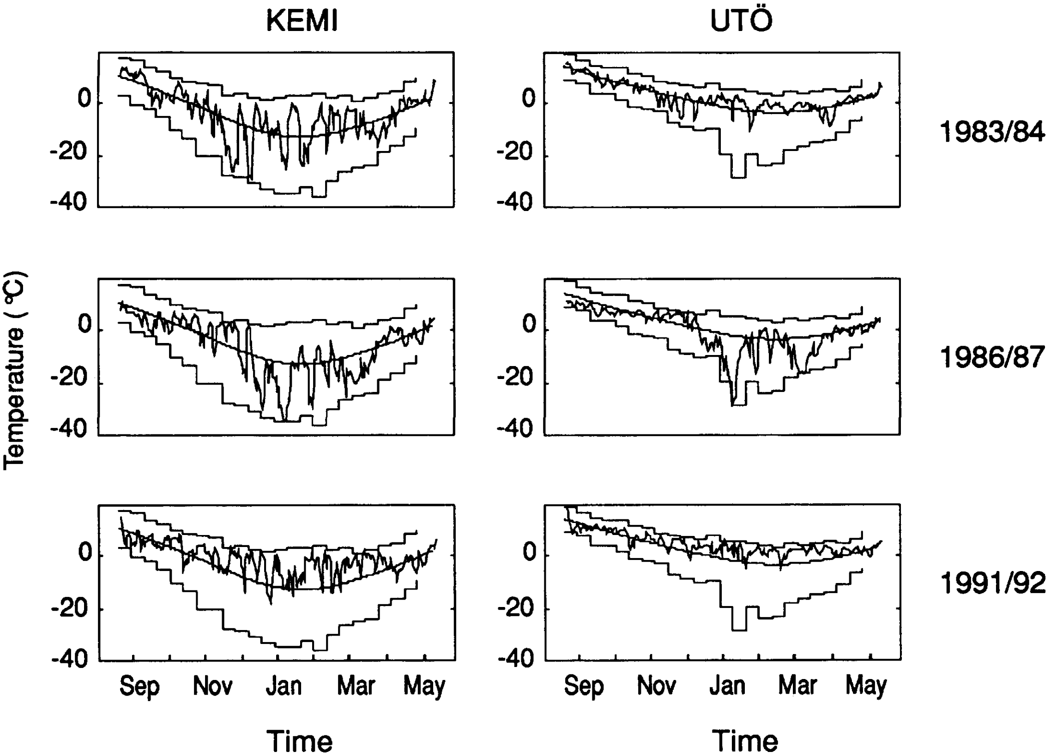

Fig. 4. Daily mean air temperature at Kemi and Utö during the winters 1983/84, 1986/87 and 1991/92. The smooth curve is the three term Fourier curve of the 1961–1990 mean temperature and the outermost curves represent the maximum and minimum values of the 1961–1990 period.

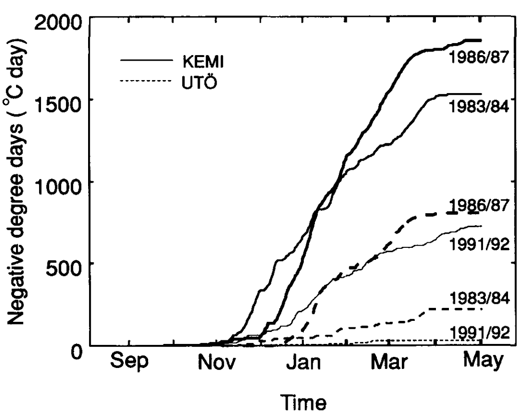

Fig. 5. Sum of negative degree days at Kemi and Utö during the ice season 1983/84, 1986/87 and 1991/92.

clearly the difference between the ice seasons in Kemi and Utö and also the disparity between the selected ice seasons. The total negative degree-day sums were 1500 °C day, 1850 °C day and 720 °C day in Kemi the during winter 1983/84, 1986/87 and 1991/92, respectively. The corresponding values for Utö are 220 °C day, 800 °C day and 30 °C day. Looking at the time evolution, we notice that the beginning of the ice season 1983/84 was colder than in 1986/87. The severity of the winter 1986/87 becomes more evident only in January 1987, especially at Utö.

3.1. *Ice season 1983/84*

The winter 1983/84 was normal. Mean air temperatures were close to the climatological mean, and colder and milder periods occurred evenly. The whole of the Gulf of Bothnia, the Gulf of

Finland and the Gulf of Riga were frozen. Freezing began in mid-November in the Bothnian Bay and in January in the Gulf of Finland. The maximum ice extent occurred on 23 March 1984, when 45% of the Baltic Sea area was ice-covered. The maximum ice thickness was 76 cm at Kemi. The fast ice broke up at Kemi in mid-May, and all the ice in the Bothnian Bay had melted by the 5th of June (Kalliosaari and Seinä, 1987).

3.2. *Ice season 1986/87*

The winter 1986/87 was considerably colder than average, January 1987 in particular being very cold. October and November 1986 were, however, warmer than average (Fig. 4). During this winter almost the whole Baltic became frozen, only the southern part of the Baltic Proper remaining open. Freezing began in December in the Bothnian Bay. By the middle of January, the Bothnian Sea, the Gulf of Finland, as well as the coastal areas of the Southern Baltic Sea, were frozen. The Kattegat and the Belt Sea were also frozen during January but the Baltic Proper remained open. In February the ice conditions weakened in the Southern Baltic Sea. Another cold period occurred in March, and the ice field became thicker; the ice cover in the Baltic Proper also began to expand. The maximum ice extent occurred on 16 March 1987, at which time only four per cent of the Baltic Sea area was ice-free. After that the areal coverage of ice reduced rapidly due to wind packing. Ice break-up occurred in the Southern Baltic at the end of March, at Utö on 20 April and at Kemi on 25 May. The maximum measured fast ice thickness was 105 cm at the Bothnian Bay, 92 cm at Kemi and 69 cm at Utö (Seinä and Kalliosaari, 1991).

3.3. *Ice season 1991/92*

During the winter 1991/92 air temperatures were almost continuously above the mean. At Utö there were only a few days with air temperatures below zero. Only the Bothnian Bay was ice-covered. Freezing began at Kemi on 18 December 1991. The maximum ice extent occurred on 21 February and then the ice coverage was only 16 per cent of the Baltic Sea area. The maximum ice thickness was 50 cm at Kemi and the final disappearance of ice occurred on 15 May 1992 (Seinä, 1996).

4. Simulated ice seasons

The aim of the present model simulations is to examine the model's ability to reproduce the observed ice season evolution. Beginning from the same initial conditions and using the observed meteorological forcing, the normal, severe and mild ice seasons were simulated. The effect of the initial temperature and salinity fields on model results is always problematic in long-term simulations. In principle, before the actual model simulations are carried out, the model should run for a time sufficiently long to dissipate the influence of the initial conditions. For practical reasons the ice seasons were simulated separately. For each season the model simulation was begun on 1 May and continued through to 31 May of the following year. Physically, the previous winter and the spring temperatures might have effect on the ice conditions of the following winter. However, a time series analysis has shown that consecutive winters are not correlated (Leppäranta and Seinä, 1985). The 6 months spin-up integration before the actual freezing date was considered long enough, e.g., Omstedt (1990) has simulated the ice season of 1986/87, and in that work the actual model simulation began on 1 November 1986. The reason for beginning the simulations in spring is because at that time, on average, the Baltic Sea has a minimum of heat storage. Thus the model calculates the gaining and releasing of heat during the summer and autumn.

A brief test on the effect of the initial temperature on the model results was made. Three simulations with a one-dimensional version of the model were made and the initial surface temperature was set equal to 1.0 °C higher than the climatological mean value, climatologial mean value and 0 °C. In a shallow water (depth <30 m) the effect of the perturbation is seen at temperature distribution about 2–3 months, but ice quantities were same in all simulations. The initial conditions for the deep areas are much more problematic (depth >100 m). The effect on the modelled surface temperature is seen 3–4 months. In the autumn and winter the surface temperatures were practically same in the all sensitivity runs. The effect is larger for the deeper layers. The sensitivity simulations showed that the initial temperature anomaly travels in the water column; the first simulation months the anomaly diffuses in the deeper model layers and during the autumn and winter it comes to the surface. The disappearance of the temperature anomaly depends highly on the surface boundary conditions and the vertical mixing coefficient, which both vary in time and space. The heat flow from the deeper layers to surface did not have any effect on the ice freezing date but could cause about 5 cm difference for the maximum ice thickness.

Model results were compared to the observed sea surface temperature, freezing date, ice thickness, compactness, and ice break-up as published by the Finnish Institute of Marine Research (FIMR). The shortage of observed data in a digitized form imposes some restrictions on the model verification. Basically, the regularly published data from the coastal fast ice region and the annual maximum ice extent reports are the only exact sources for the ice conditions. The observed freezing date, the maximum ice thickness and the ice break-up date at Kemi and Utö are listed in Table 2 (Kalliosaari and Seinä, 1987; Seinä and Kalliosaari, 1991; Seinä, 1996). For the model verification we took simulation results from the nearest grid point. The modelled freezing date and ice break-up date are defined to be those moments in time when the initial freezing and the final ice disappearance have occurred. In the comparison we have to take into consideration that the observed values are single point measurements, while the model values represent an average over a model grid cell ($10' \times 20'$). For the drift ice field the only verification material is based on the published ice charts. Visual comparison with the ice charts has been used in the model development phase. Here we show only the observed and modelled ice situations at the time of occurrence of the maximum ice extent. To show the evolution of the modelled sea surface temperature and ice thickness we selected two model grid points to represent the Bothnian Sea and the Bothnian Bay.

The verification of the ice dynamics is not presented here. A case study showed the ability of the model to reproduce realistic ice velocity fields (Leppäranta et al., 1995). In that work the real ice field displacements were obtained from consecutive ERS-1 SAR images for three periods during the winter 1994. The observed ice velocity fields were realistically simulated using plastic ice rheology, and the large-scale compressive strength was found to be $2.5 \cdot 10^4$ Nm^{-2}.

4.1. Sea surface temperature and freezing date

The evolution of the modelled ocean surface temperature and ice thickness are shown in Figs. 6a–e during the three test ice seasons. The model gives a realistic annual cycle of the surface temperature, and the differences between the three test years are clearly seen. However, temperatures in the summer period are underestimated, while for the autumn the model gives surface temperatures about 1–1.5 °C higher than those shown in the published ice charts. Close to the freezing point (0–1 °C) the simulated temperatures are consistent with the observations.

The model produces characteristics in the evolution of the ice seasons which are quite similar to those occurring in nature (Table 2). In the Southern Baltic the sea freezes only in severe ice winters, the Gulf of Finland and the Gulf of Bothnia are frozen in average ice winters and the Bothnian Bay is frozen over in every winter. The freezing dates were close to those observed. At Kemi the differences between the observed and modelled freezing dates are within 7 days. In the winter 1983/84 the first occurrence of the ice at Utö was on 25 January 1984 but permanent ice cover formed only on 7 March, which is close to the modelled freezing date at 11 March. For the ice winter 1986/87 the modelled freezing date is delayed five days compared with the observations.

The modelled and observed ocean surface temperature fields at the date of occurrence of the observed annual maximum ice extent are shown in Figs. 7a, b–9a, b. The modelled ice edge is well reproduced for 1983/84 (Fig. 7a, b). There is a warm spot in the modelled surface temperature: in the central parts of the Bothnian Sea the temperature is 0.0–0.5 °C while it should be at the freezing point. The surface temperature in the central parts of the Baltic proper is overestimated in the model by about 1 °C.

In the ice season of 1986/87 (Fig. 8a) almost all Baltic Sea surface waters were at the freezing point in mid-March, but the model still had too much heat content in the deeper parts of the Baltic. The modelled temperatures for the Central Baltic Sea

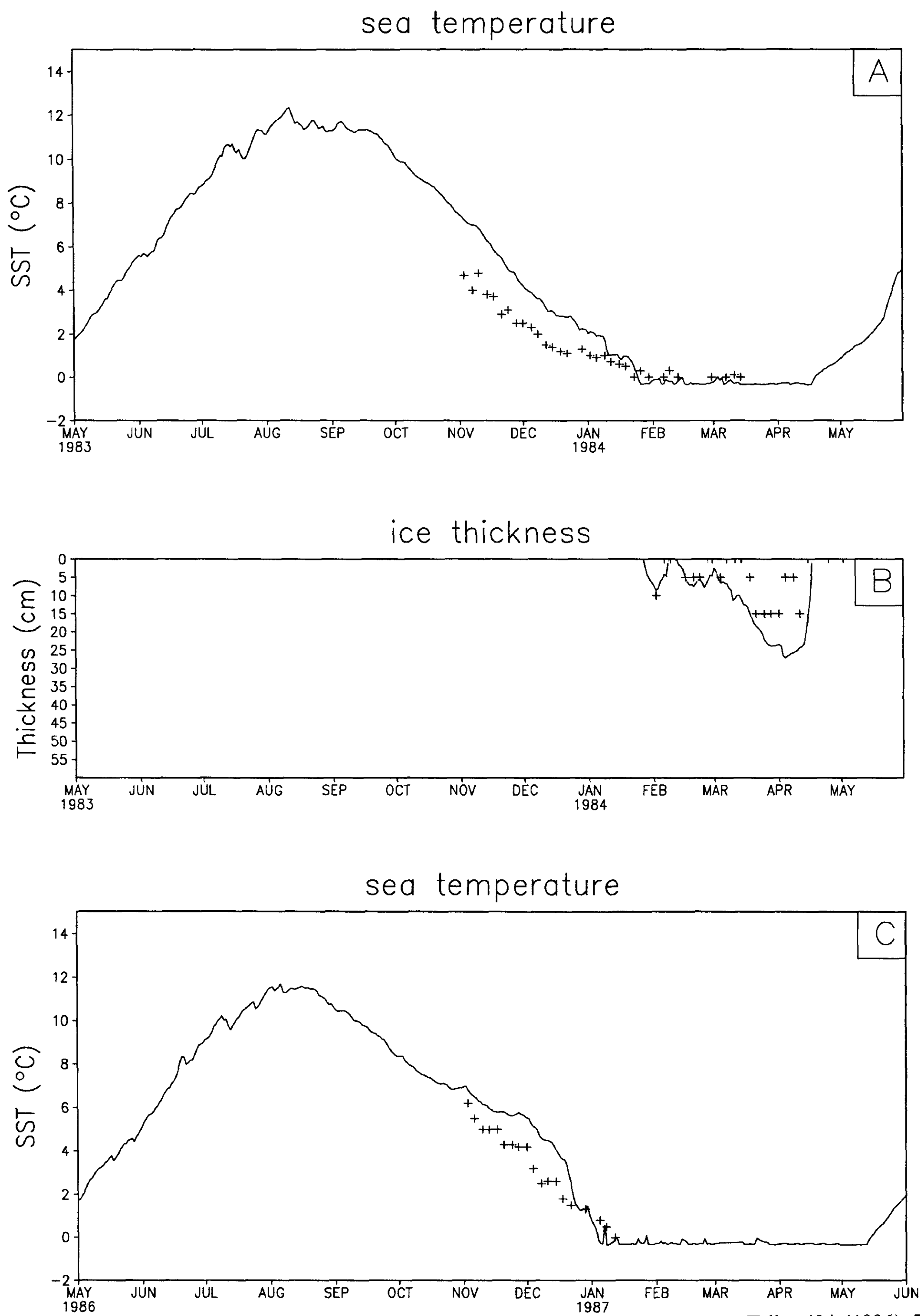
sea temperature
A
SST (°C)
MAY 1983
JUN
JUL
AUG
SEP
OCT
NOV
DEC
JAN 1984
FEB
MAR
APR
MAY
ice thickness
B
Thickness (cm)
MAY 1983
JUN
JUL
AUG
SEP
OCT
NOV
DEC
JAN 1984
FEB
MAR
APR
MAY
sea temperature
C
SST (°C)
MAY 1986
JUN
JUL
AUG
SEP
OCT
NOV
DEC
JAN 1987
FEB
MAR
APR
MAY
JUN

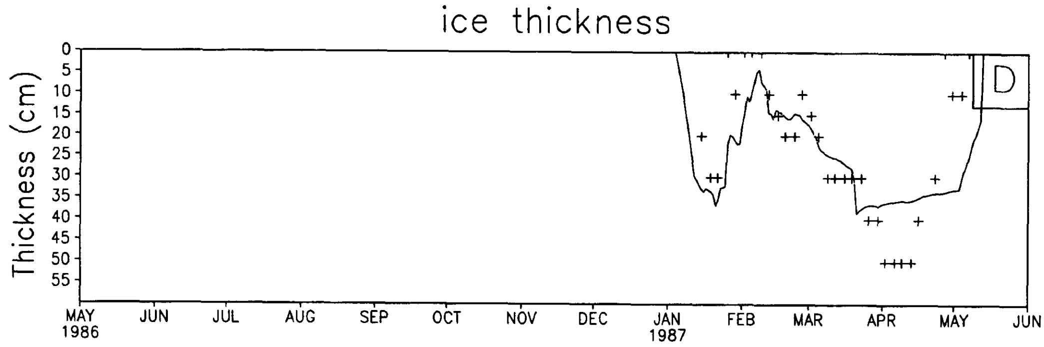

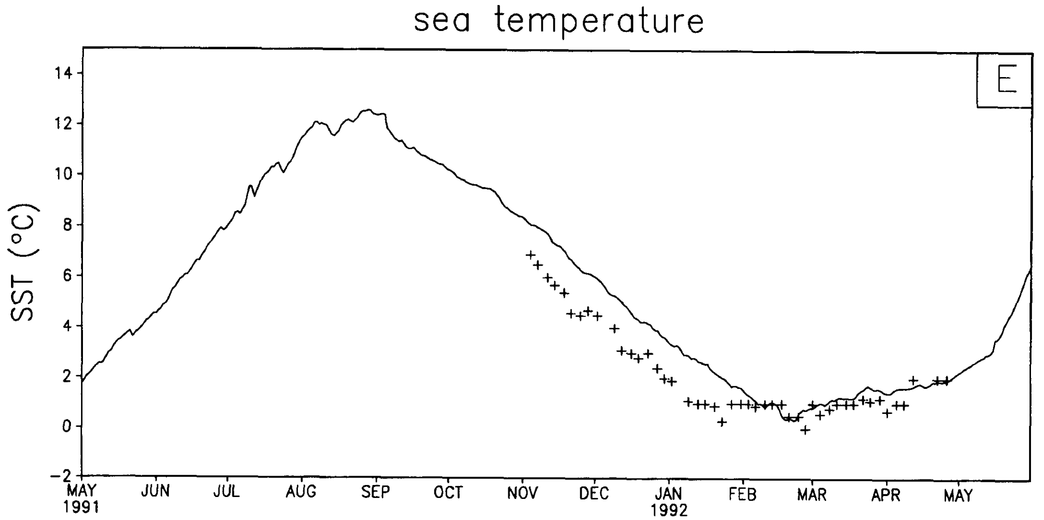

Fig. 6. Simulated surface temperature and ice thickness evolution for the Bothnian Sea (lat = 61°, lon = 18°) during the periods (ab) 1 May 1983–31 May 1984, (cd) 1 May 1986–31 May 1987 and (e) 1 May 1991–31 May 1992. The crosses indicate the observed values obtained from the ice charts (FIMR).

were as high as 0.5–2.5 °C. In 1991/92 most of the Baltic Sea was open and the model reproduced sea surface temperature well (Fig. 9a, b). The ice edge was as observed. Also the surface temperatures in shallow areas were consistent with the observations; the deep central parts of the Bothnian Sea and the Baltic Proper were, on the other hand, about 1 °C too warm.

The reason for the excessively warm ocean surface layer in deep areas might be the crude parametrization of the vertical mixing or too coarse vertical resolution of the model. The vertical grid step is about 25–50 m in the deep areas. The heat content of such a water column is large, and it responds only slowly to the surface fluxes. However, we have made model experiments with a slab ocean model and in these simulations the ocean surface layer was cooled too rapidly, resulting in a large overestimation of the total ice mass.

4.2. *Ice thickness and break-up*

The ice thickness results for Kemi are shown in Fig. 10. Generally, the ice thickness evolution is well simulated in the model, particularly during the early stage of ice growth. The maximum ice thickness is overestimated by about 10 cm in the

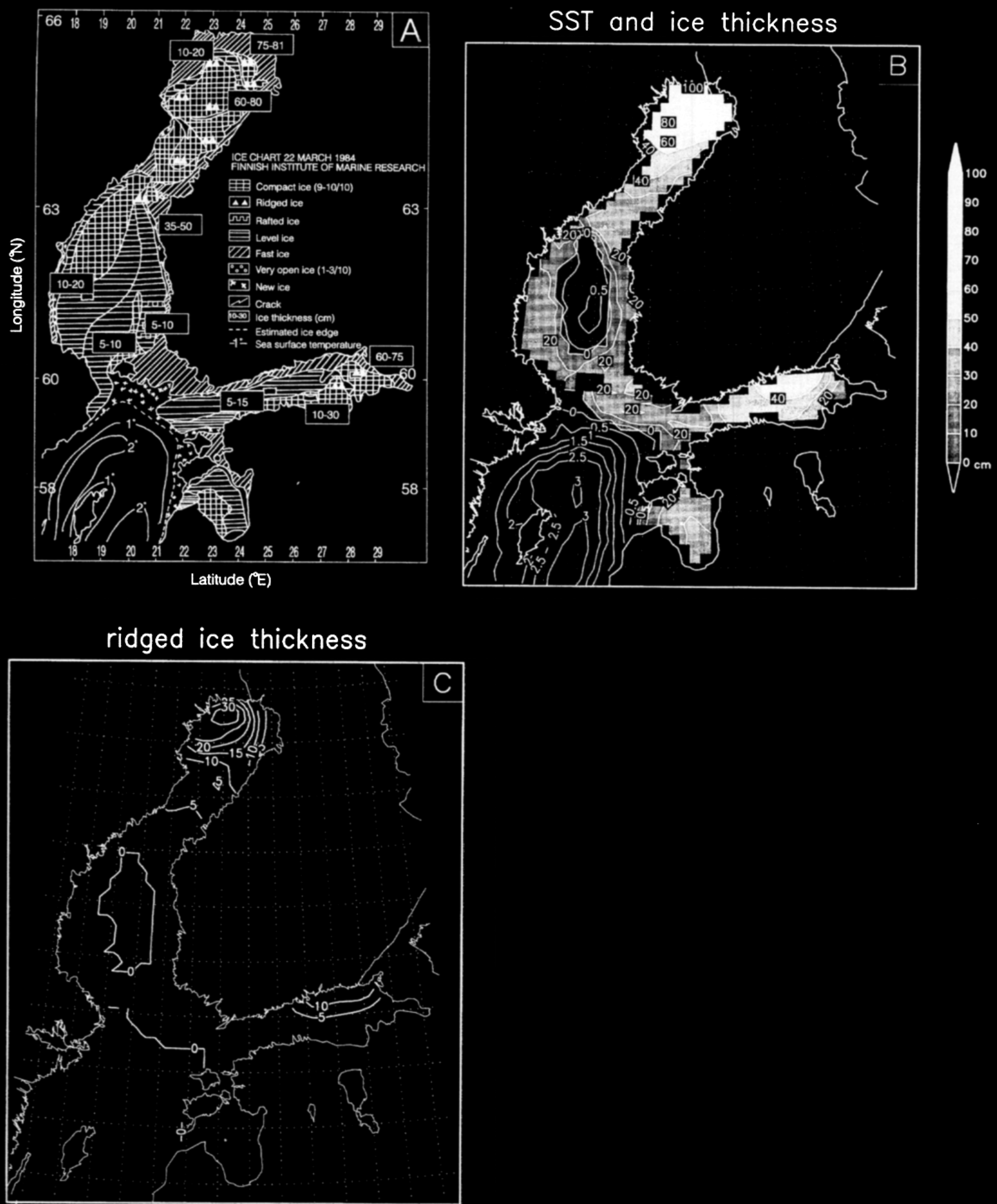

Fig. 7. Observed ice conditions and sea surface temperature (a) and modelled sea surface temperature and total ice thickness (b) and ridged ice thickness (c) on 22 March 1984. In the panel (b) the contour in the shaded area are ice thickness contour (cm) and the contour in the blank area are temperatures (°C).

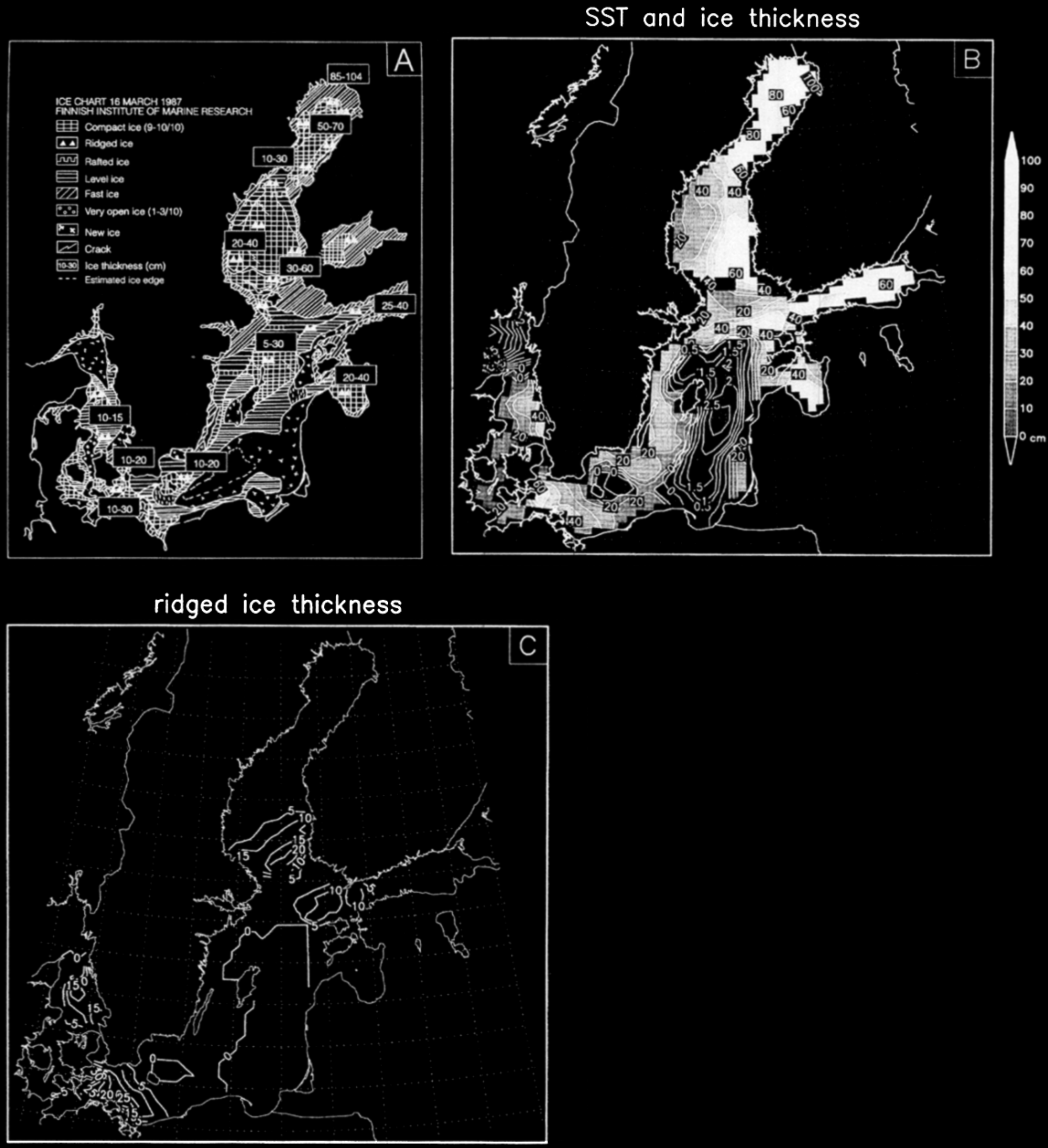

Fig. 8. Observed ice conditions and sea surface temperature (a) and modelled sea surface temperature and total ice thickness (b) and ridged ice thickness (c) on 16 March 1987. In the panel (b) the contour in the shaded area are ice thickness contour (cm) and the contour in the blank area are temperatures (°C).

winters 1983/84 and 1986/87 (Table 2); however, ice thicknesses over one metre were observed in the some other measurement sites near Kemi (Kalliosaari and Seinä, 1987; see also Fig. 8a). The ice thickness difference may arise due to snow thickness or oceanic heat flux differences. In spring the ice melting rate is about the same as is observed, but the beginning of the ice melting is delayed in the simulation results. This leads to about two weeks delay in the ice break-up date (Table 2). The delay in the ice melting may be due to the parametrization of the surface albedo and

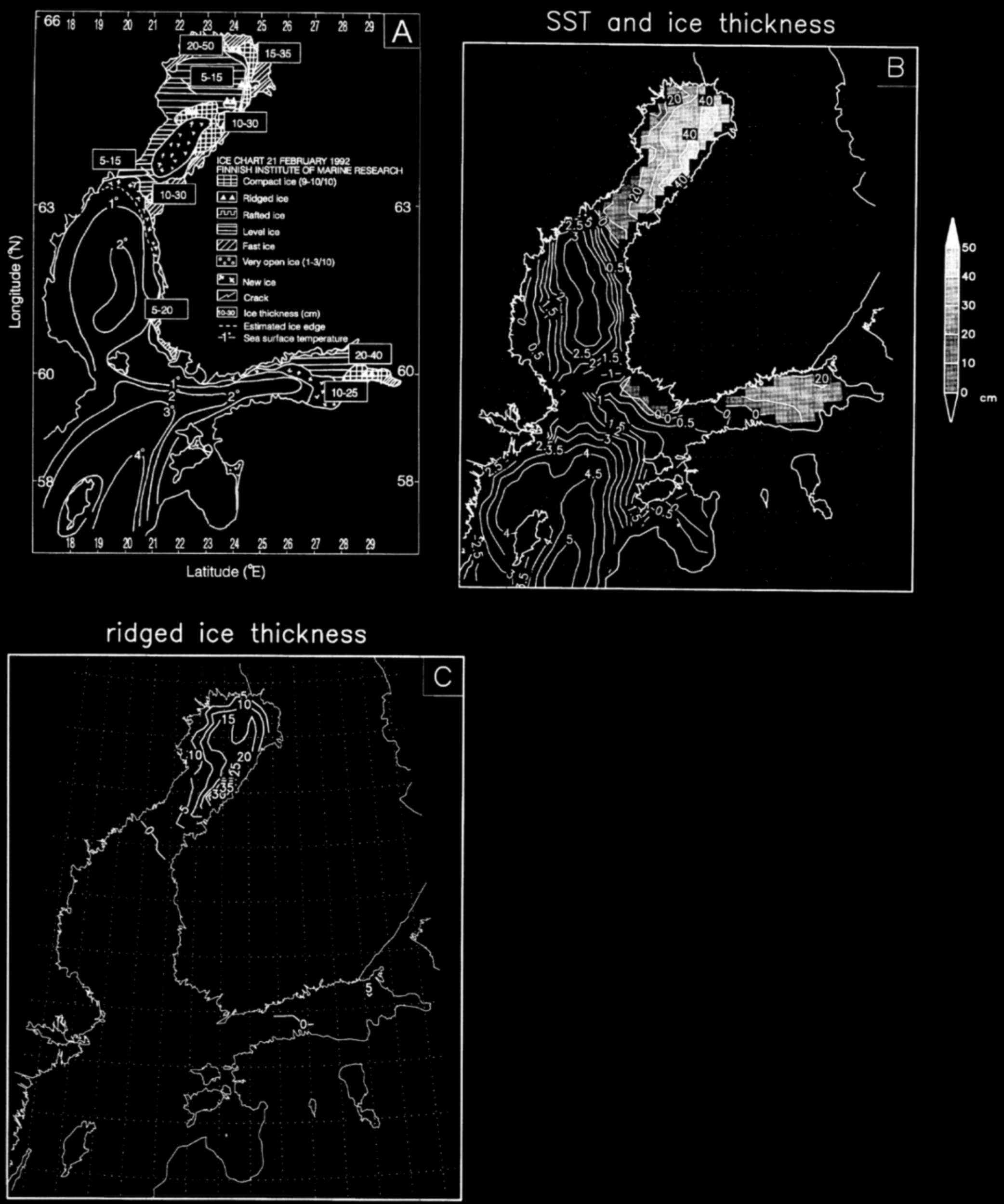

Fig. 9. Observed ice conditions and sea surface temperature (a) and modelled sea surface temperature and total ice thickness (b) and ridged ice thickness (c) on 21 February 1992. In the panel (b) the contour in the shaded area are ice thickness contour (cm) and the contour in the blank area are temperatures (°C).

also because the solar radiation penetration into ice and the internal melting of the ice were not taken into account.

The evolution of the simulated ice thickness is also realistic in the drift ice areas (Figs. 6b, d). In addition to the fairly smooth thermodynamic ice growth and decay, sudden changes in the simulated ice thickness due to the ice dynamics are apparent in the simulation results. In the Bothnian Bay, where the thermodynamic growth is larger and the ice pack is less mobile than in the other basins, the thermodynamic growth was a more dominating feature in the ice thickness time series. The ice dynamic effects (advection and deformation) are much more clearly seen in the time series for the Bothnian Sea (Figs. 6b, d). The sudden ice disappearance after the initial freezing was observed both in 1984 and 1987. Those events are revealed in the model results as well.

The modelled ice thickness fields are shown in Figs. 7b–9b for the time of the maximum ice extent. The overall structure of the ice thickness fields is produced rather well but the ice edge region is biased. On 23 March 1984 the simulated ice thickness is 40–100 cm in the Bothnian Bay, while the ice chart gives an ice thickness range of 10–81 cm (Fig. 7a). In the Bothnian Sea, the range of ice thickness is 10-30 cm in the model and 5–20 cm in the observed data. In the Gulf of Finland and in the Gulf of Riga the simulated ice thickness is 10–40 cm while the observed values are 5–30 cm.

The dynamic build-up is described by the distribution of the ridged ice thickness (Figs. 7c–9c). The verification of these thicknesses against ice charts is only qualitative. The locations of the heavily ridged areas are indicated by the black triangles in the ice charts. In 1983/84 the main ridging areas are at the fast ice boundary in the Bothnian Bay and the Gulf of Finland (Fig. 7a), which are also realized in the model (Fig. 7c). The modelled ridged ice thickness is 5–30 cm which is statistically the correct range (Lewis et al., 1993).

The simulated ice thickness field is very well in agreement with observations in the Bothnian Bay, the Bothnian Sea and in the Gulf of Finland at the time of the maximum ice extent in the winter 1986/87 (Fig. 8a, b). The maximum simulated ice thickness is about 100 cm in the northern fast ice zone, while the observed maximum is 104 cm. In the Bothnian Sea the both thickness fields are in the range 20–60 cm. Even some sub-basin scale features are realized in the thickness distribution in the Bothnian Sea: according to the ice chart the ice thickness increases towards the Finnish coast, which is reproduced also in the model results. In the Gulf of Finland the simulated ice thickness is 40–60 cm but the observed values are less, 25–40 cm. The agreement is good in the Gulf of Riga: 20–40 cm for simulated and observed ice thicknesses. For the Kattegat and the Southern Baltic Sea the model slightly overestimates ice thickness. The model gives 30–50 cm, observations 10–30 cm. The ridging areas in the Southern Bothnian Sea, Western Gulf of Finland and in the Western Baltic Proper come out well, but for the Bothnian Bay the model fails to produce ridged ice (Figs 8a, c).

In the ice season 1991/92, the overall features in ice thickness field are fairly well simulated (Fig. 9a, b). The model-derived ice thickness in the Bothnian Bay is 10–40 cm; the observed thickness is 5–50 cm. In the Gulf of Finland the simulated ice thickness is about 10–20 cm, while the ice chart reports an ice thickness of 10–40 cm. The model-produced ridged ice along the Finnish coast in the Bothnian Bay is also shown in the ice chart.

4.3. *Ice extent*

Figs. 7a, b–9a, b show that the model-produced ice extent agrees well with the observations at the time of occurrence of the maximum ice extent. The time series of the simulated ice extent are shown in Fig. 10. The difference between the ice seasons is clearly seen. At the early phase of ice season 1983/84 the ice extent was actually larger than in the severe ice season 1986/87 due to the relatively cold periods in November and December 1984 (Figs. 4, 5). In January 1987 the ice area increased rapidly, while the growth of ice extent during the winter 1983/84 was rather steady.

The modelled times of occurrence of the annual maximum ice extent are quite close to the dates observed (Table 2). A slight delay is found, which is partly due to the broad maximum of the calculated ice extent (Fig. 11). This is particularly the case for the ice winter 1991/92. The simulated maximum ice extent and the simulated ice extent on the date of the observed maximum are almost the same. In the normal and severe winters the predicted ice extent is about 20% less than that

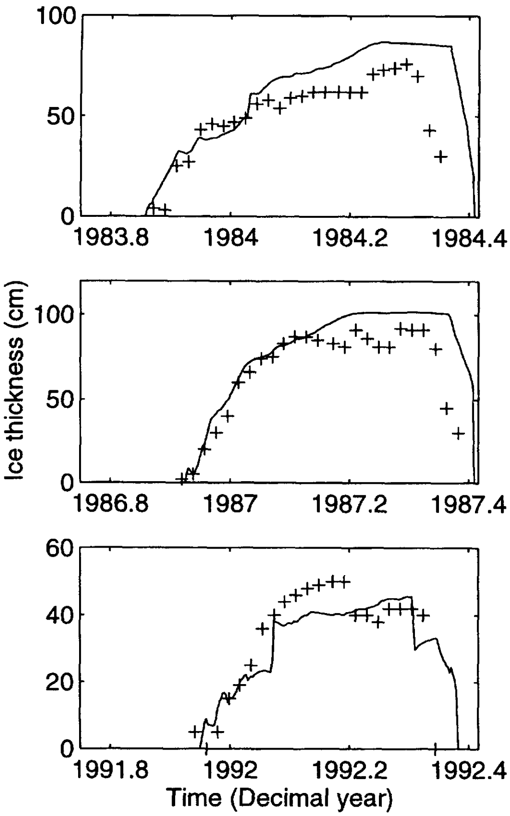

Fig. 10. Observed and modelled ice thickness in Kemi during the ice season 1983/84, 1986/87 and 1991/92.

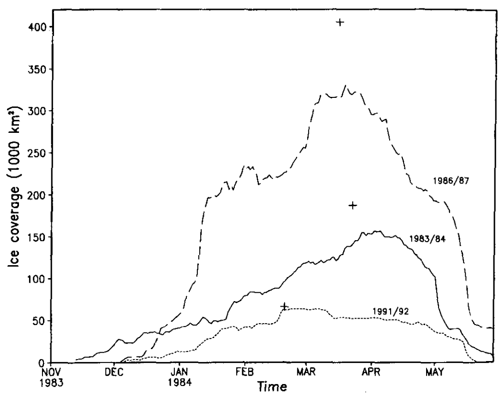

Fig. 11. Simulated ice coverage of the total Baltic Sea area during 1 Nov 1983–31 May 1984, 1 Nov 1986–31 May 1987 and 1 Nov 1991–31 May 1992. Crosses indicate the observed annual maximum ice extent.

observed, while in the mild winter the modelled and observed ice extent are practically the same. The differences for the winters 1983/84 and 1986/87 arise mainly from deeper parts of the basins where the modelled ocean surface temperatures are too high (Figs. 7b–9b).

The disappearance of the ice cover takes place stepwise (Fig. 11). At first the Baltic Proper becomes ice free, then the Bothnian Sea and the Gulf of Finland, and finally the Bothnian Bay. The model simulations show some ice left even at the end of May. According to the observations, the last ice did not melt until the beginning of June in the winters 1983/84 and 1986/87 (Kalliosaari and Seinä, 1987; Seinä and Kalliosaari, 1991).

4.4. *Surface layer heat content*

The modelled heat content of the surface layer in the Bothnian Bay, the Bothnian Sea and in the Baltic Proper is largely related to the total volume of the surface layer. The different heat storages of the sub-basins are evident and the difference between the average, cold and warm winters is also reproduced in the model simulations. At the beginning of November the heat content of the Bothnian Bay is about $10 \cdot 10^{19}$ J. In the Bothnian Sea it is $\sim 30 \cdot 10^{19}$ J and in the Baltic Proper around $110 \cdot 10^{19}$ J. The Bothnian Bay loses practically all its heat storage during all the simulated winters. During the average and cold winters the Bothnian Sea also uses up its heat content completely, but during the mild winter the minimum heat content is still $10 \cdot 10^{19}$ J. The Baltic Proper loses its heat content at a higher rate than the other basins. The minimum of heat content occurs in March, when it is still $20\text{–}60 \cdot 10^{19}$ J.

The change of the heat content of the surface layer is due the surface heat and radiation balance, horizontal advection and vertical mixing. During the autumnal cooling and winter stages the main driving factor is the atmosphere-ocean heat exchange. During the cooling period the heat change is ~ -100 Wm^{-2}. During the ice-covered period the heat change is almost zero, or even slightly positive in the Bothnian Bay due to heat advection and mixing. The largest modelled cooling is over -300 Wm^{-2}, occurring in the middle of January 1987. This peak is seen in both the Bothnian Sea and the Baltic Proper time series, being due to a cold easterly airflow over the Baltic Sea. The Baltic Proper was ice-free and relatively warm, a factor which caused heavy snowfall in the coastal areas of Sweden. The episode has been analyzed and modelled by Andersson and Gustafsson (1994) with respect to the generation of convective snowbands.

5. Concluding remarks

A new seasonal coupled ice-ocean model for the Baltic Sea has been presented. The evolution of the ice season has been simulated for three particular seasons, normal (1983/84), severe (1986/87) and mild (1991/92). The model results were compared to the observed sea surface temperature, freezing date, ice thickness and compactness and ice break-up, as available from the published ice charts and tables. The conclusions are as follows.

It has been shown that the main characteristics of the ice season could be reproduced by a moderate resolution ice-ocean model. Beginning from the same initial conditions and using the observed meteorological forcing, the model simulated realistic annual cycles of sea surface temperature, ice thickness and coverage and described the interannual variability of the ice season well.

The most important factor controlling the ice edge and initial freezing in the model is the proper modelling of the ocean surface layer. It determines the heat content of the surface layer and hence the freezing date. In these simulations the ocean surface layer was simulated well in the shallow sea areas. The simulated surface temperatures over the deeper central parts of the basins were systematically too warm in the winter stage. This may be due to too coarse vertical resolution in the model and to the simple parametrization scheme of the vertical mixing. To solve this problem the ice model should be coupled to an eddy-resolving three-dimensional ocean model, and the coupling should probably be handled with a boundary-layer model for calculating more accurate fluxes between ice and ocean. However, those models are computationally still too time-consuming for climate simulations.

The ice growth was simulated realistically. However, the maximum ice thicknesses were slightly larger than observed. The overestimation may be due to an underestimation of snow thickness and oceanic heat flux. The beginning of the ice melting was delayed, which led to about two weeks delay in the ice break-up date. The delayed ice melting may be due to the parametrization of the surface albedo and also because the penetration of the solar radiation into the ice was not taken into account.

Dynamic produced ridged ice thickness fields were qualitatively correct. The modelled locations of the ridged areas were in consistency with the ice chart information and modelled ridged ice thickness of 5–30 cm corresponds the observed range. For this study ice velocity fields were not available for the verification, but it is expected that satellite SAR data will provide much better material for ice dynamic research during the next few years.

Further development of the present model needs more observations for its validation. Ice pack redistribution processes, penetration of the solar radiation into the ice, and the snow cover over the ice are both poorly understood and not properly taken into account in present-day ice-ocean models. Extensive observation of the ice thickness and drift are required at a basin size and on the seasonal scale. At present, ice thickness data are obtained from fast ice sites and point ship observations. For modelling purposes grid cell scale mean values would be much more useful. The prescribed atmosphere used in these simulations controls the results largely and the coupling the ice-ocean model to an atmospheric model is required in future. To understand and model the winter season is one of the key issues of the BALTEX programme (BALTEX, 1995): its model-oriented field campaign will give much useful data for the development of coupled atmosphere-ice-ocean models.

Acknowledgements

Fruitful discussion with Anders Omstedt and Timo Vihma and their comments on the manuscript were valuable. We also thank the anonymous reviewers for their constructive criticism and Robin King for the language corrections. Bundesamt für Seeschiffahrt und Hydrographie, Deutscher Wetterdienst, the Estonian Meteorological and Hydrological Institute, the Finnish Institute of Marine Research, the Finnish Meteorological Institute, the Hydrometeorological Observatory of Klaipeda, the Institute of Meteorology and Water Management, the Latvian Hydrometeorological Agency and the Swedish Meteorological and Hydrological Institute are thanked for providing meteorological and hydrological data for this study. The Finnish Center for Scientific Computing is acknowledged for computing facilities provided on the CRAY-C94. This work is financed by the Academy of the Finland under the Finnish research program on Climate Change (SILMU).

REFERENCES

Alenius, P. and Makkonen, L. 1981. Variability of the annual maximum ice extent of the Baltic Sea. *Arch. Met. Geophys. Bioklim.* **29**, 396–398.

Andersson, T. and Gustafsson, N. 1994. Coast of departure and coast of arrival: two important concepts for the formation and structure of convective snowbands over ses and lakes. *Mon. Wea. Rev.* **122**, 1036–1049.

BALTEX, 1995. *Baltic Sea Experiment BALTEX. Initial Implementation Plan.* International BALTEX Secretariat, GKSS Research Center, Geestacht, Germany, Pub. 2, 84pp.

Budyko, M. I. 1974. *Climate and life.* Academic Press, 508pp.

Fofonoff, N. P. 1985. Physical properties of sea water: a new salinity scale and equation of state for seawater. *J. Geophys. Res.* **90**, 3332–3342.

Haapala, J. and Alenius, P. 1994. Temperature and salinity statistics for the Northern Baltic Sea 1961–90. *Finnish Marine Research* **262**, 51–121.

Haapala, J., Alenius, P., Dubra, J., Klyachkin, S. V., Kôuts, T., Leppäranta, M., Omstedt, A., Pakstys, L., Schmelzer, N., Schrum, C., Seinä, A., Strübing, K., Sztobryn, M. and Zaharchenko, E. 1996. IDA, Ice data bank for Baltic Sea climate studies. University of Helsinki, Dept. of Geophysics. *Report series in Geophysics* **35**, 45pp.

Hibler, W. D. 1979. A dynamic thermodynamic sea ice model. *Journal of Physical Oceanography* **9**, 815–846.

Hibler, W. D. 1986. Ice dynamics. In: *The geophysics of sea ice*, ed. N. Untersteiner. The Nato ASI series, B 146. Plenum, USA, 577–640.

Ikeda, M. 1988. A three-dimensional coupled ice-ocean model of coastal circulation. *J. Geophys. Res.* **93**, 10731–10748.

Iqbal, M. 1983. *An introduction to solar radiation.* Academic Press, 390pp.

Kantha, L. H. and Mellor, G. L. 1989. A two-dimensional coupled ice-ocean model of the Bering Sea marginal ice zone. *J. Geophys. Res.* **94**, 10921–10935.

Kalliosaari, S. and Seinä, A. 1987. Ice winters 1981–1985 along the Finnish coast. *Finnish Marine Research* **254**, 1–63.

Koslowski, G. and Loewe, P. 1994. The western Baltic sea ice season in terms of mass-related severity index: 1879–1992, Part I. Temporal variability and association with the north Atlantic oscillation. *Tellus* **46A**, 66–74.

Kowalik, Z. and Murthy, T. S. 1993. Numerical modeling of ocean dynamics. *Advanced Series on Ocean Engineering* **5**. World Scientific, 481pp.

Lehmann, A. 1995. A three-dimensional baroclinic eddy resolving model of the Baltic Sea. *Tellus* **47A**, 1013–1031.

Leppäranta, M. 1981a. An ice drift model for the Baltic Sea. *Tellus* **33**, 583–596.

Leppäranta, M. 1981b. On the structure and mechanics of pack ice in the Bothnian Bay. *Finnish Marine Research* **248**, 3–86.

Leppäranta, M. and Omstedt, A. 1990. Dynamic coupling of sea ice and water for an ice field with free boundaries. *Tellus* **42A**, 482–495.

Leppäranta, M. and Seinä, A. 1985. Freezing, maximum annual ice thickness and break up of ice on the Finnish coast during 1830–1984. *Geophysica* **21**, 87–104.

Leppäranta, M., Yan, S. and Haapala, J. 1995. Comparison of sea ice velocity fields from ERS-1 SAR and a dynamic model. In: Yan Sun (ed.): *SAR remote sensing.* Technical report 275, Chalmers University of Tecnology, Gothenburg, Sweden.

Lewis, J. E., Leppäranta, M. and Granberg, H. B. 1993. Statistical properties of sea ice surface topography in the Baltic Sea. *Tellus* **45A**, 127–142.

Maykut, G. A. 1986. The surface heat mass balance. In: *The geophysics of sea ice,* ed.: N. Untersteiner. The Nato ASI series, B 146. Plenum, USA, 395–464.

Millero, F. J. 1978. Freezing point of sea water, Eighth report of the joint panel on oceanographic tables and standards. *UNESCO Technical Papers in Marine Science* **28**, UNESCO, Paris, France.

Mysak, L. A., Ingram, R. G., Wang, J. and van der Baaren, A. 1996. The anomalous sea ice extent in Hudson Bay, Baffin Bay and the Labrador Sea during three simultaneous NAO and ENSO episodes. *Atmosphere-Ocean*, in press.

Omstedt, A., 1990. Modelling the Baltic Sea as thirteen sub-basins with vertical resolution. *Tellus* **42A**, 286–301.

Omstedt, A. and Nyberg, L., 1996. Responce of Baltic sea ice to seasonal, interannual forcing and climate change. *Tellus* **48A**, this issue.

Omstedt, A., Nyberg, L. and Leppäranta, M. 1994. *A coupled ice-ocean model supporting winter navigation in the Baltic Sea.* Part 1. *Ice dynamics and water levels.* Swedish Meteorological and Hydrological Institute, RO 17, 17pp.

Omstedt, A., Sahlberg, J. and Svensson, U. 1983. Measured and numerically-simulated autumn cooling in the Bay of Bothnia. *Tellus* **35A**, 231–240.

Omstedt, A. and Wettlaufer, J. S. 1992. Ice growth and oceanic heat flux, models and measurements. *J. Geophys. Res.* **97**, 9383–9390.

Overland, J. E. and Pease, C. H. 1988. Modeling ice dynamics of coastal seas. *J. Geophys. Res.* **93**, 15619–15637.

Perovich, D. K. 1996. The optical properties of sea ice. *CRREL Monograph,* **96**–1. Hanover, NH, USA.

Reed, R. K., 1977. An estimating insolation over the ocean. *J. Phys. Oceanogr.* **7**, 482–485.

Rogers, J. C. 1984. The association between the North Atlantic Oscillation and the Southern Oscillation in the northern hemisphere. *Mon. Wea. Rev.* **112**, 1999–2015.

Seifert, T. and Kayser, B. 1995. A high resolution spherical grid topography of the Baltic Sea. Institut für Ostseeforschung, Warnemünde. *Marine Science Reports* **9**, 74–88.

Seinä, A. and Kalliosaari, S. 1991. Ice winters 1986–1990 along the Finnish coast. *Finnish Marine Research* **259**, 3–61.

Seinä, A. 1996. Ice season 1991–1995 along the Finnish coast. *Finnish Marine Research,* in press.

SMHI and FIMR, 1982. *Climatological ice atlas for the Baltic Sea, Kattegat, Skagerrak and Lake Vänern (1963–1979).* Norrköping, 220pp.

Semtner, A. J. 1976. A model for the thermodynamic growth of sea ice in numerical investigations of climate. *J. Phys. Oceanogr.* **6**, 379–389.

Stigebrandt, A. 1987. A model for the vertical circulation of the Baltic deep water. *J. Phys. Oceanogr.* **17**, 1772–1785.

Wang, J., Mysak, L. A., Ingram, R. G. 1994a. A numerical simulation of sea ice cover in Hudson Bay. *J. Phys. Oceanogr.* **24**, 2515–2533.

Wang, J., Mysak, L. A., Ingram, R. G. 1994b. Interannual variability of sea-ice cover in Hudson Bay, Baffin Bay and Labrador Sea. *Atmosphere-Ocean* **32**, 421–447.

Zhang, Z. and Leppäranta, M. 1995. Modeling the influence of ice on sea level variations in the Baltic Sea. *Geophysica* **31**, 31–45.